RSC Advances




ROYAL SOCIETY OF CHEMISTRY

www.rsc.org/advances

# Incorporation of Graphene Oxide into $C_{12}E_4$/$C_{12}$mimBr Hybrid Lyotropic Liquid Crystal and its Thermo-Sensitive Properties

Lin Wang, Xia Xin *, Mengzhou Yang, Jinglin Shen, Shiling Yuan *

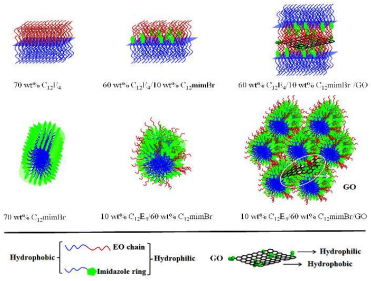


Schematic illustration of the formation of GO/$C_{12}E_4$/$C_{12}$mimBr lamellar and hexagonal LLC composites.

*Author to whom correspondence should be addressed, E-mail: xinx@sdu.edu.cn.

Phone: +86-531-88363597. Fax: +86-531-88361008

*Author to whom correspondence should be addressed, E-mail: shilingyuan@sdu.edu.cn.

Phone: +86-531-88365896. Fax: +86-531-88564750

# Incorporation of Graphene Oxide into $C_{12}E_4$/$C_{12}$mimBr Hybrid Lyotropic Liquid Crystal and its Thermo-Sensitive Properties

Lin Wang [a], Xia Xin [a, b *], Mengzhou Yang [a], Jinglin Shen [a], Shiling Yuan [a *]

[a] *Key Laboratory of Colloid and Interface Chemistry (Shandong University), Ministry of Education, Shanda nanlu No. 27, Jinan, 250100, P. R. China*

[b] *National Engineering Technology Research Center for Colloidal Materials, Shandong University, Shanda nanlu No. 27, Jinan, 250100, P. R. China*



[*]Author to whom correspondence should be addressed, E-mail: xinx@sdu.edu.cn.

Phone: +86-531-88363597. Fax: +86-531-88361008

[*]Author to whom correspondence should be addressed, E-mail: shilingyuan@sdu.edu.cn.

Phone: +86-531-88365896. Fax: +86-531-88564750

**Abstract**

Graphene oxide (GO) was successfully incorporated into a hybrid lyotropic liquid crystal (LLC) matrix formed by two kinds of surfactants n-dodecyl tetraethylene monoether ($C_{12}E_4$) and 1-dodecyl-3-methylimidazolium bromide ionic liquid ($C_{12}$mimBr). By changing the ratios of $C_{12}E_4$ and $C_{12}$mimBr, two types of $C_{12}E_4$/$C_{12}$mimBr LLC matrixes (lamellar and hexagonal phase) were formed and the effects of the concentration of GO and temperature on the properties of GO/$C_{12}E_4$/$C_{12}$mimBr LLC composites were systematically investigated by polarized optical microscopy (POM) observations, small-angle X-ray scattering (SAXS) and rheological measurement. Both POM observations and SAXS results indicated that GO can be well-dispersed in the hybrid LLC matrixs at room temperature. Moreover, after the incorporation of GO, the temperature tolerance of GO/$C_{12}E_4$/$C_{12}$mimBr LLC composites were enhanced compared with pure $C_{12}E_4$/$C_{12}$mimBr hybrid LLC and aggregated GO was not observed in the $C_{12}E_4$/$C_{12}$mimBr LLC hybrid hexagonal matrix with the increase of temperature while it can be observed in the $C_{12}E_4$/$C_{12}$mimBr LLC hybrid lamellar matrix. The results of rheological measurements showed that the addition of GO were helpful for enhancing the mechanical properties of $C_{12}E_4$/$C_{12}$mimBr LLC. Thus, the success preparation of GO/hybrid LLC composites can highly improve the thermal stability of these materials and widen the applications of GO/LC materials in nanotechnology, electrochemical, drug delivery systems and bioengineering areas.

## Introduction

Lyotropic liquid crystal (LLC) is a special kind of the self-assembly of amphiphilic molecules within the scope of the long range ordered arrangement, and its unique functions cannot be replaced by other materials.[1-3] LLC can be used as a template to synthesize or assemble nonfunctional materials, which has received widespread attention.[4-8] As we all known, the structure of LLC matrix can be regulated by changing its composition such as the type of amphiphilic molecules, the concentration, the solvent conditions, etc. Except for traditional surfactants, long-chain alkyl ionic liquids are special kinds of amphiphilic surfactant molecules which can also form LC. Ionic liquids are often moderate to poor conductors of electricity, non-ionizing, highly viscous and frequently exhibit low vapor pressure.[9] In addition the other properties are diverse due to their purely ionic character, such as low combustibility, excellent thermal stability, wide liquid regions, and favorable solvating properties.[10-12] Therefore, long-chain alkyl-imidazollium ionic liquids has become hotspots in research fields due to its rich phase behavior.[13-15] For example, Zhang et al. investigated the phase behavior of $C_8$mimCl/$H_2O$/alcohols (1-hexanol, 1-octanol, 1-decanol, and 1-dodecanol) at 25°C, the lamellar phases were found in all systems, and the length of alkyl chain of alcohols on the impact of LLC structures were also discussed.[16] Moreover, Zhang et al. also compared two ternary systems $C_{16}$mimBr/$H_2O$/$C_{10}H_{21}OH$ and CTAB/$H_2O$/$C_{10}H_{21}OH$, and investigated the effect of hydrophilic group on the structure of LLC and finally got the formation mechanism of complex crystal.[17]

Long-chain alkyl ionic liquids/traditional surfactants mixed systems can enrich the variety of LLC matrix and offer a new way for their application.[18] Moreover, it is also interesting to build orderly organic/inorganic hybrids by doping nanoparticles (especially with special property, such as

optical, electrical, magnetic and biocompatibility) into LLC matrix. In addition to showing the nature of every component of these hybrids, new features were also exhibited duo to the interaction between those components.[19-21] As a special carbon material, graphene is the one with the most potential due to its outstanding physical, chemical and electronic properties.[22] Graphene oxide (GO) is a graphene sheet with carboxylic groups at its edges and phenol, hydroxyl and epoxide groups on its basal plane which makes it can be dispersed in water by simple ultrasonication and became a material with good hydrophilic and biocompatible properties.[23, 24] Those groups can be also combined with small organic molecules by hydrogen bonds and π-π bonds which induce GO-LLC composites has potential applications in drug release and dye adsorbtion.[25-27] For example, Sun et al. incorporated GO into PNIPAM hydrogel by one-step strategy and their PNIPAM-*co*-AA microgels showed dual thermal and pH response with good reversibility.[28] In our previous work, a detailed survey has been carried out on GO/$C_{12}E_4$-LLC composites.[20] Furthermore, we incorporated CNTs into LLC matrix formed by nonionic surfactant or ionic surfactant through spontaneous phase separation process, respectively, and the properties of CNTs-nonionic surfactant and CNTs-ionic surfactant were compared.[29, 30]

In this paper, GO was successfully incorporated into a hybrid LLC matrix formed by nonionic surfactant n-dodecyl tetraethylene monoether ($C_{12}E_4$) and long-chain alkylimidazollium ionic liquids 1-dodecyl-3-methylimidazolium bromide ($C_{12}$mimBr). The properties of GO/$C_{12}E_4$/$C_{12}$mimBr LLC composites were systematically investigated by polarized optical microscopy (POM) observations, small-angle X-ray scattering (SAXS) and rheological measurement. Compared with LC formed by single non-ionic surfactant, it is expected that the hybrid LC may be have a better property of thermal stability due to less influence of temperature

changes of ionic liquids, so the effects of temperature on the properties of GO/$C_{12}E_4$/$C_{12}$mimBr LLC composites were investigated. Moreover, it can be concluded that the liquid crystal composite formed by ionic liquids $C_{12}$mimBr and the traditional surfactant $C_{12}E_4$ enriched the variety of liquid crystal template.

## Experimental

### Chemicals

Nonionic surfactant ($C_{12}E_4$) was purchased from Acros Organics (USA) and the purity was greater than 99%. Long-chain alkylimidazollium ionic liquids ($C_{12}$mimBr) was purchased from Lanzhou institute of chemical physics with the purity greater than 99%. GO (diameter: 0.5–5μm, thickness: 0.8–1.2 nm) was obtained from Nanjing XFNANO Materials Tech Co., Ltd. All the above reagents were used without further purification. Water used in the experiments was triply distilled using a quartz water purification system.

### Methods and characterization

GO (25 mg) is added into water (5 mL) directly by ultrasonication for 4 h, then stock GO dispersion was obtained and can stand for at least two weeks. Sample preparation: The total mass fraction of solute ($C_{12}E_4$ and $C_{12}$mimBr) was 70 wt%, the solvent is water or a dispersion of GO, samples were prepared by mixing the substances with a certain amount.

TEM observations were carried out on a JEOL JEM-100 CXII (Japan) at an accelerating voltage of 80 kV and about 5 μL of solution was placed on a TEM grid and the excess solution was wicked away with filter paper. Field-emission scanning electron microscopy (FE-SEM) observations were carried out on a JSM-6700F. For the sample preparation, a drop of GO dispersion was placed on a silica wafer to form a thin film. The wafers were freeze-dried in a vacuum extractor at −55 °C.

Small-angle X-ray scattering (SAXS) observations were carried out on a HMBG-SAX X-ray small-angle scattering system (Austria) with a Ni-filtered Cu Kα radiation (0.154 nm) operating at 50 kV and 40 mA. The distance between the sample and detector was 27.8 cm. Polarized microscopy observations were carried out on AXIOSKOP 40/40 FL (ZEISS, Germany) microscope and Nikon Eclipse E400 microscope equipped with a LINKAM THMS 600 heating/cooling stage.

The rheological measurements were carried out on an Anton Paar Physica MCR302 rheometer with a plate-plate system (diameter, 25 mm; 0°). In oscillatory measurements, an amplitude sweep at a fixed frequency was performed prior to the following frequency sweep in order to ensure that the selected stress was in the linear viscoelastic region. The viscoelastic properties of the samples were determined by oscillatory measurements in the frequency range of 0.01-100 Hz. The samples were measured at 20.0 ± 0.1 °C with the help of a cyclic water bath.

**Results and discussion**

**Dispersion states of graphene oxide**

TEM and SEM images of the freeze-dried 5 mg $mL^{-1}$ GO dispersion were shown in Figure 1. The TEM image of GO (Figure 1A) shows that it contains several graphitic layers and some place of it fold to induce wrinkles. For the SEM image (Figure 1B), a 3D film network structure was observed and GO sheets appeared in a loose pore structure which is due to the force balance between electrostatic repulsion and binding interactions (hydrogen bonding, π-stacking, hydrophobic effect, etc.).[31] Then, the GO dispersion was diluted to the desired concentration for later use.

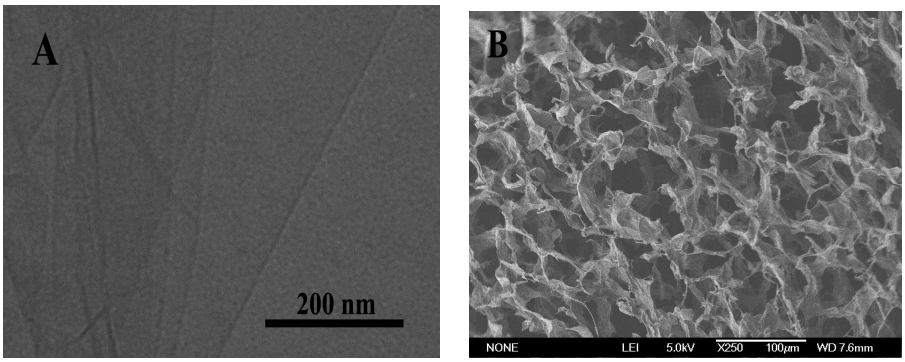


**Figure 1** TEM (A) and SEM (B) images of freeze-dried of 5 mg·mL$^{-1}$ GO solution.

**Phase behavior of hybrid $C_{12}E_4$/$C_{12}$mimBr LC composites**

First, the phase behavior of $C_{12}E_4$/$C_{12}$mimBr mixed system was investigated by fixing the total concentration of $C_{12}E_4$ and $C_{12}$mimBr at 70 wt% and changing the ratio of $C_{12}E_4$ and $C_{12}$mimBr. The SAXS results are shown in Figure 2. It can be seen that two peaks were detected for all the samples. The relative position ratio of these two peaks for the samples a-d was 1:2 when the concentration of $C_{12}$mimBr is below 30 wt% which is expected for the (001) and (002) reflections of the lamellar phase. A samples e was not an uniform phase by macroscopic observation, and the SAXS results also showed that it was not a lamellar or hexagonal phase, so we have not do further research about it. When the concentration of $C_{12}$mimBr exceeds 50 wt%, the relative position ratio of these two peaks for the samples f-h changed to 1: $\sqrt{3}$ which is expected for the (001) and (002) reflections of the hexagonal phase.[32-34] Thus, it can be concluded that the phase state of $C_{12}E_4$/$C_{12}$mimBr hybrid composites can be controlled by changing the ratio of $C_{12}E_4$ and $C_{12}$mimBr. On the basis of the above results, the sample b which represents the lamellar phase and the sample g which represents the hexagonal phase, respectively, were selected as the templates for the further study.

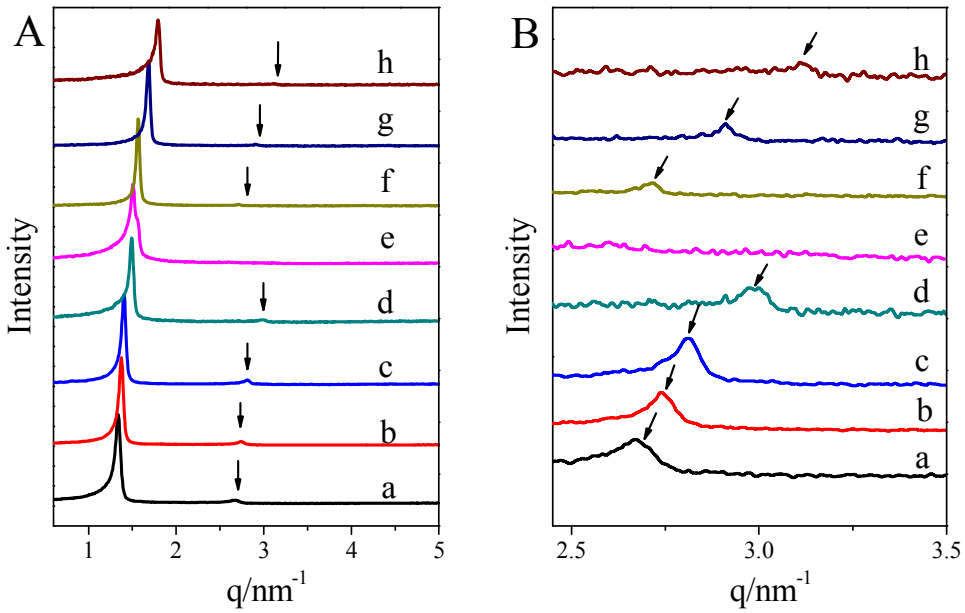


**Figure 2** SAXS results (A) and (B) the amplification part of 2.45-3.5 $nm^{-1}$. a) 70 wt% $C_{12}E_4$, b) 60 wt% $C_{12}E_4$/10 wt% $C_{12}$mimBr, c) 50 wt% $C_{12}E_4$/20 wt% $C_{12}$mimBr, d) 40 wt% $C_{12}E_4$/30wt% $C_{12}$mimBr, e) 30 wt% $C_{12}E_4$/40 wt% $C_{12}$mimBr, f) 20 wt% $C_{12}E_4$/50 wt% $C_{12}$mimBr, g) 10 wt% $C_{12}E_4$/60 wt% $C_{12}$mimBr and h) 70 wt% $C_{12}$mimBr.

**The effect of $C_{GO}$ on the properties of GO/$C_{12}E_4$/$C_{12}$mimBr LLC composites**

POM images of the above hybrid LLC composites were shown in Figure 3. Figure 3 (A-D) showed the POM results of pure $C_{12}E_4$/$C_{12}$mimBr LLC while Figure 3 (a-d) showed the results of GO/$C_{12}E_4$/$C_{12}$mimBr LLC composites. Under POM observations, it can be seen that samples of (A, a, B, b) showed maltese crosses which are characteristic of lamellar structures, and samples of (C, c, D, d) showed fan-like texture which are characteristic of hexagonal structures. Compared the POM images of $C_{12}E_4$/$C_{12}$mimBr LLC with and without GO, it can be found that the textures of these composites were similar, indicating that GO were well-incorporated into $C_{12}E_4$/$C_{12}$mimBr LLC matrix without destroy their structures.[35, 36]

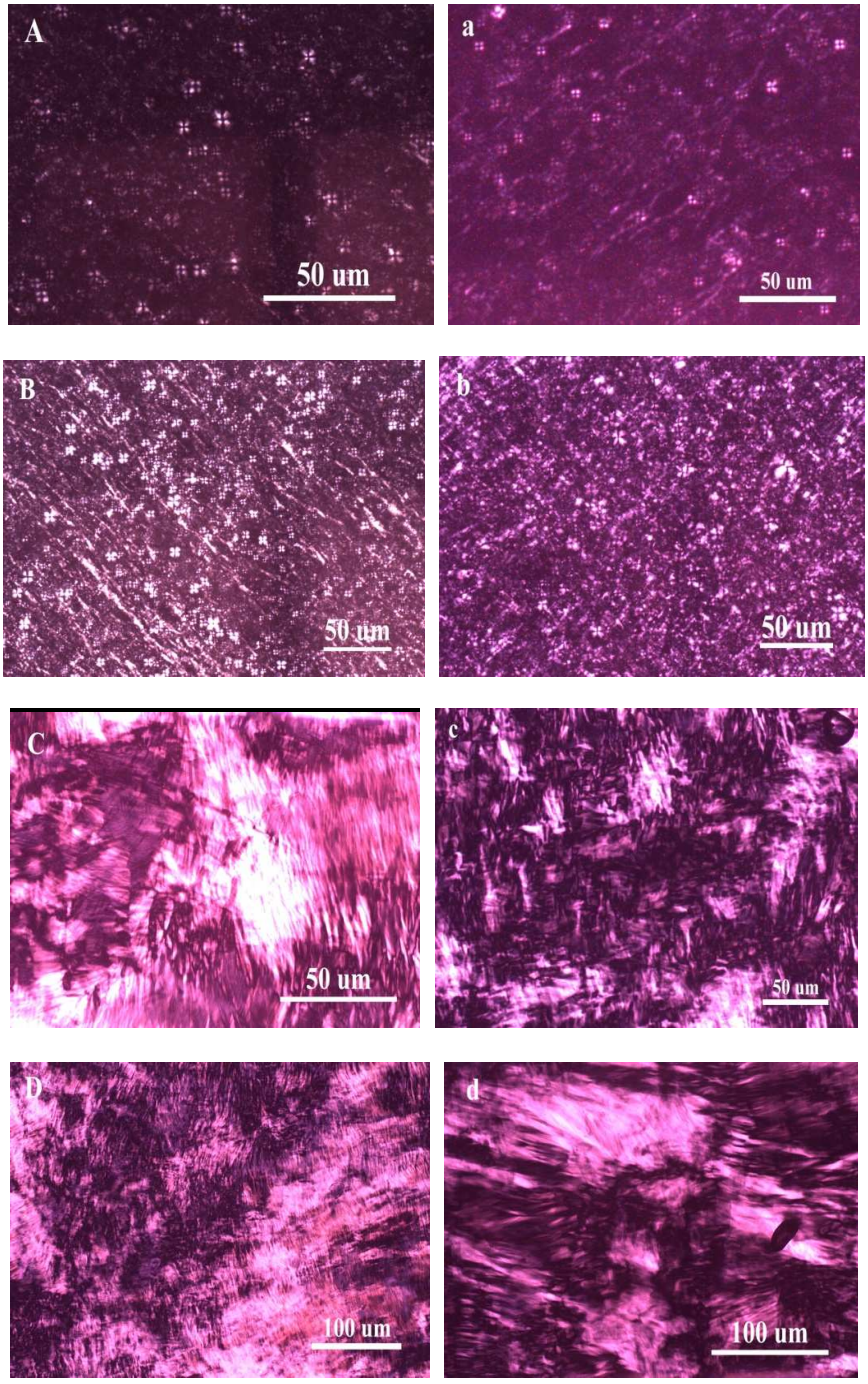


**Figure 3** POM images of LLC matrix without GO. A) 70 wt% $C_{12}E_4$, B) 60 wt% $C_{12}E_4$/10 wt% $C_{12}$mimBr, C) 10 wt% $C_{12}E_4$/60 wt% $C_{12}$mimBr and D) 70 wt% $C_{12}$mimBr. POM image of composites with GO. a) 70 wt% $C_{12}E_4$, b) 60 wt% $C_{12}E_4$/10 wt% $C_{12}$mimBr, c) 10 wt% $C_{12}E_4$/60 wt% $C_{12}$mimBr and d) 70 wt% $C_{12}$mimBr.

To further obtain the details about the phase behaviors of GO/$C_{12}E_4$/$C_{12}$mimBr LLC composites, SAXS measurements were carried out. Figure 4 A showed the variation of SAXS results of 60 wt% $C_{12}E_4$/10 wt% $C_{12}$mimBr LLC composites as a function of the concentration of GO ($c_{GO}$), two peaks were detected with a relative position ratio of 1:2 which respected the lamellar phase. Moreover, the position of the peaks moved to left a bit with the increasing of $c_{GO}$. The *d*-spacing of the lamellar lattice was calculated by $d = 2\pi/q_1$ ($q_1$ was the value of the first peak). It was found that the *d*-spacing of the lamellar lattice were increased from 4.33 nm to 4.76 nm as $c_{GO}$ increases. Figure 4B s showed the variation of SAXS results of 10 wt% $C_{12}E_4$/60 wt% $C_{12}$mimBr LLC composites as a function of $c_{GO}$, two peaks were detected with a relative position ratio of 1: $\sqrt{3}$ which respected the hexagonal phase. The *d*-spacing of hexagonal phase was calculated by $d = 4\pi/(q_1)$ ($q_1$ was the value of the first peak). Interestingly, it can be seen that with the increase of $c_{GO}$, the *d*-spacing remained nearly the same (~ 4.29 nm). It was clearly observed that the *d*-spacing of lamellar phase was larger than the hexagonal phase which may be because of the length of the imidazole ring shorter than EO chain (Figure 4 C).

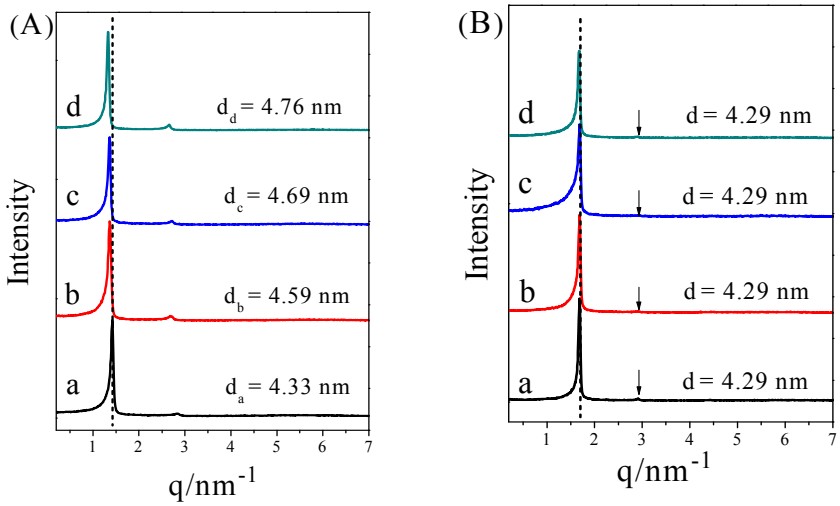

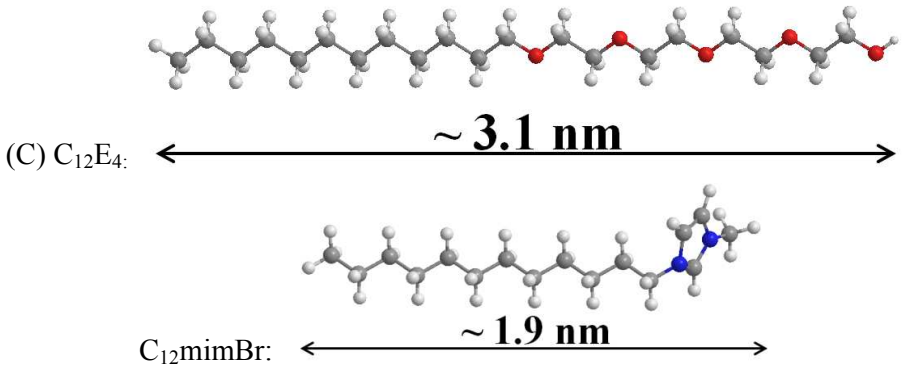


**Figure 4** The results of SAXS, A) lamellar liquid crystal (60 wt% $C_{12}E_4$/10 wt% $C_{12}$mimBr), B) hexagonal liquid crystal (10 wt% $C_{12}E_4$/60 wt% $C_{12}$mimBr). The concentration of GO were a) 0 mg·mL$^{-1}$, b) 0.3 mg·mL$^{-1}$, c) 0.6 mg·mL$^{-1}$ and d) 0.9 mg·mL$^{-1}$. (C) The structure and the length of $C_{12}E_4$ and C12mimBr. Color code for atoms: blue, nitrogen; red, oxygen; dark gray, carbon; light gray, hydrogen.

Rheological measurements can give macro properties of the system in real-time and then reflect the change of internal microstructure; thus, it is an important method to investigate LLC materials.[37, 38] We compared the properties of GO/$C_{12}E_4$/$C_{12}$mimBr LLC composites between lamellar phase and hexagonal phase and the results are shown in Figure 5. The stress sweep test was executed at a fixed frequency of 1.0 Hz (Figure 5A, a), a critical stress value (yield stress, $\tau^*$) was appeared. The shear modulus sharply decreased above the $\tau^*$ and the system shown properties of Newtonian-like flow.[39] In addition, the addition of GO greatly increased the range of the linear viscoelastic region of both lamellar phase and hexagonal phase, and the shear modulus increased with the increasing of $c_{GO}$. For example, G′ of lamellar phase of 60 wt% $C_{12}E_4$/10 wt% $C_{12}$mimBr without GO was 2780 Pa, and the value of G′ increased progressively from 3216 Pa to 3826 Pa when $c_{GO}$ increased from 0.3 mg·mL$^{-1}$ to 0.9 mg·mL$^{-1}$. Moreover, the same phenomenon occurred with the increase of $c_{GO}$ for the hexagonal phase LLC. For example, G′ of hexagonal phase of 10 wt% $C_{12}E_4$/60 wt% $C_{12}$mimBr

LLC without GO was 84500 Pa, and the value of G′ increased progressively from 91900 Pa to 95200 Pa when $c_{GO}$ increased from 0.3 mg·mL$^{-1}$ to 0.9 mg·mL$^{-1}$.

In the whole frequency measurement, the system of both lamellar phase and hexagonal phase showed a strong elastic response (Figure 5B, b). Elastic modulus of GO/$C_{12}E_4$/$C_{12}$mimBr LLC composites also increased continuously with the increase of $c_{GO}$. For example, G′ of lamellar phase and hexagonal phase of $C_{12}E_4$/$C_{12}$mimBr LLC without GO were 2364 Pa and 163217 Pa, respectively. When $c_{GO}$ was 0.9 mg·mL$^{-1}$, the value of G′ increased to 3364 Pa and 268006 Pa, respectively. The η* of both systems decreased with the increase of frequency indicating a shear-thinning behavior (Figure 5C, c). Moreover, the value of η* increased with the increase of $c_{GO}$ which indicated that the addition of GO enhanced the mechanical property of $C_{12}E_4$/$C_{12}$mimBr LLC material.

From all of the above experimental results, it can be seen that for our systems, GO is not only used for improving mechanical properties but also $C_{12}E_4$/$C_{12}$mimBr LLC can tune the system`s morphology from lamellar to hexagonal, where the lamellar can work as a `trigger` for releasing back the GO, while hexagonal is more stable.

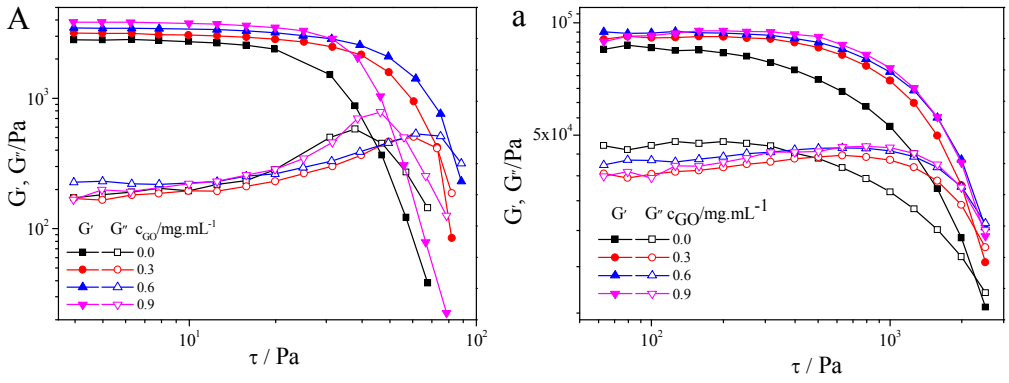

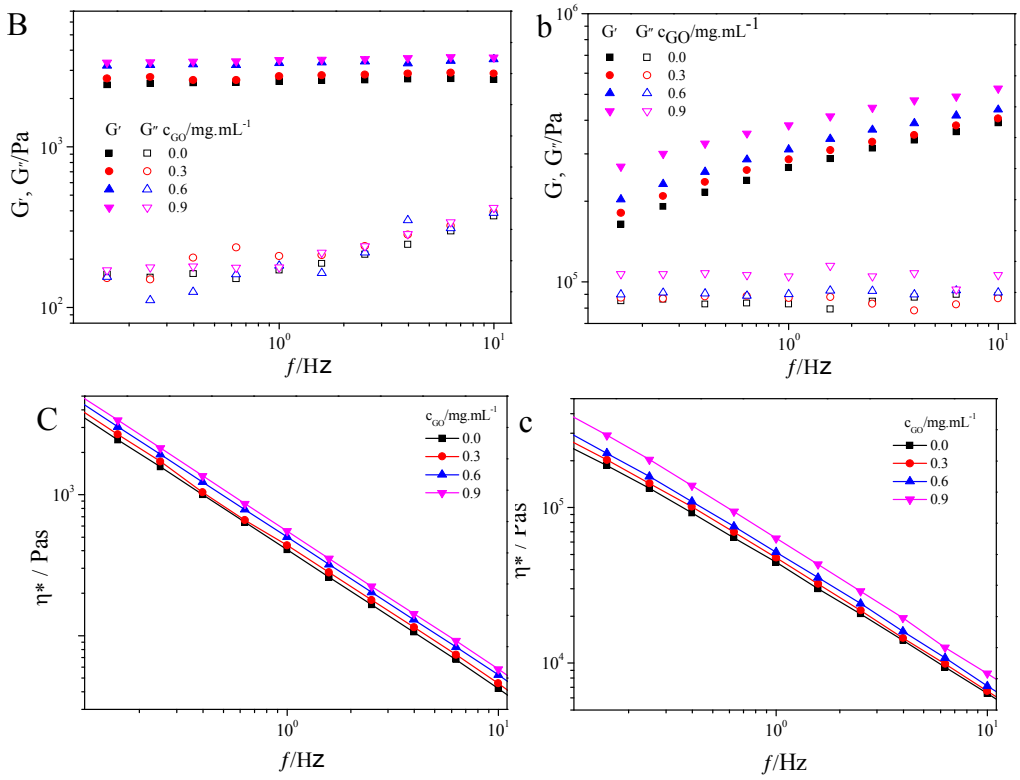


**Figure 5** Rheological properties of liquid crystal composites as a function of GO, Left) lamellar liquid crystal composites (60 wt% $C_{12}E_4$/10 wt% $C_{12}$mimBr) and Right) hexagonal liquid crystal composites (10 wt% $C_{12}E_4$/60 wt% $C_{12}$mimBr). (A), (a) G′ and G″ as a function of the applied stress (τ) at f = 1.0 Hz, (B), (b) G′ and G″ and (C), (c) η* as a function of f.

**The effect of tempareture on the properties of GO/$C_{12}E_4$/$C_{12}$mimBr LLC composites**

Cloud point is characteristic of nonionic surfactants containing polyoxyethylene chains. Nonionic surfactants exhibit reverse solubility versus temperature behavior in water and therefore "cloud out" at some point as the temperature is raised.[29, 40] So the LLC composites formed by nonionic surfactants are easy to destroy at high temperature. The variation of the SAXS results of 70 wt% $C_{12}E_4$ LLC as a function of temperature were shown in Figure 6. It can be seen that two peaks were detected with a relative position ratio of 1:2 when the temperature is below 40°C and the shape of the peaks gradually widened and disappeared when the temperature is above 40°C.

However, the peaks reappeared when the temperature returned to 20°C.

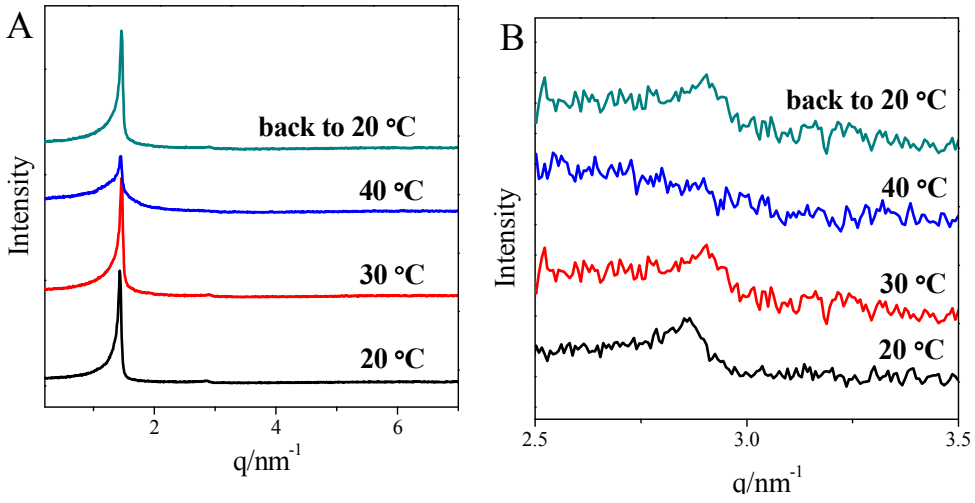


**Figure 6** (A) The variation of the SAXS results of 70 wt% $C_{12}E_4$ LLC as a function of temperature. (B) the amplification part of (A) of 2.5-3.5 $nm^{-1}$.

In order to improve the thermal stability of the LLC materials, $C_{12}$mimBr and GO were incorporated into the system. For the composites, SAXS measurements were carried out as a function of temperature (Figure 7). It can be clearly seen the addition of $C_{12}$mimBr greatly increased the thermal stability of $C_{12}E_4$ LLC. Compared 60 wt%$C_{12}E_4$/10 wt% $C_{12}$mimBr LLC with 70 wt% $C_{12}E_4$ LLC, The peaks of 60 wt% $C_{12}E_4$/10 wt% $C_{12}$mimBr LLC became wider and shorter after the temperature above 70°C as shown in Figure 7A, indicating the lamellar phase were destroyed. This temperature (70°C) is much higher than that of 70 wt% $C_{12}E_4$ (40°C). Besides, the thermal stability of the lamellar $C_{12}E_4$/$C_{12}$mimBr composites (80°C) was slightly increased with the addition of 0.3 $mg \cdot mL^{-1}$ GO. In other words, the addition of GO into $C_{12}E_4$/$C_{12}$mimBr LLC was beneficial to the increase of their thermal stability. For the hexagonal phase (10 wt% $C_{12}E_4$/60 wt% $C_{12}$mimBr LLC and 0.3 $mg \cdot mL^{-1}$ GO/10 wt% $C_{12}E_4$/60 wt% $C_{12}$mimBr LLC), when the temperature increased from 20°C to 80°C, two peaks were detected with a relative position ratio of

1: $\sqrt{3}$ and it maintained no deformation of the shape of peaks even at high temperature (Figure 7B, 7b), indicating the high thermal stability of the hexagonal $C_{12}E_4/C_{12}$mimBr LLC and GO/$C_{12}E_4/C_{12}$mimBr LLC composites. Hence, it can be concluded that the properties of the LLC materials can be controlled by adjusting the content of $C_{12}$mimBr and GO.

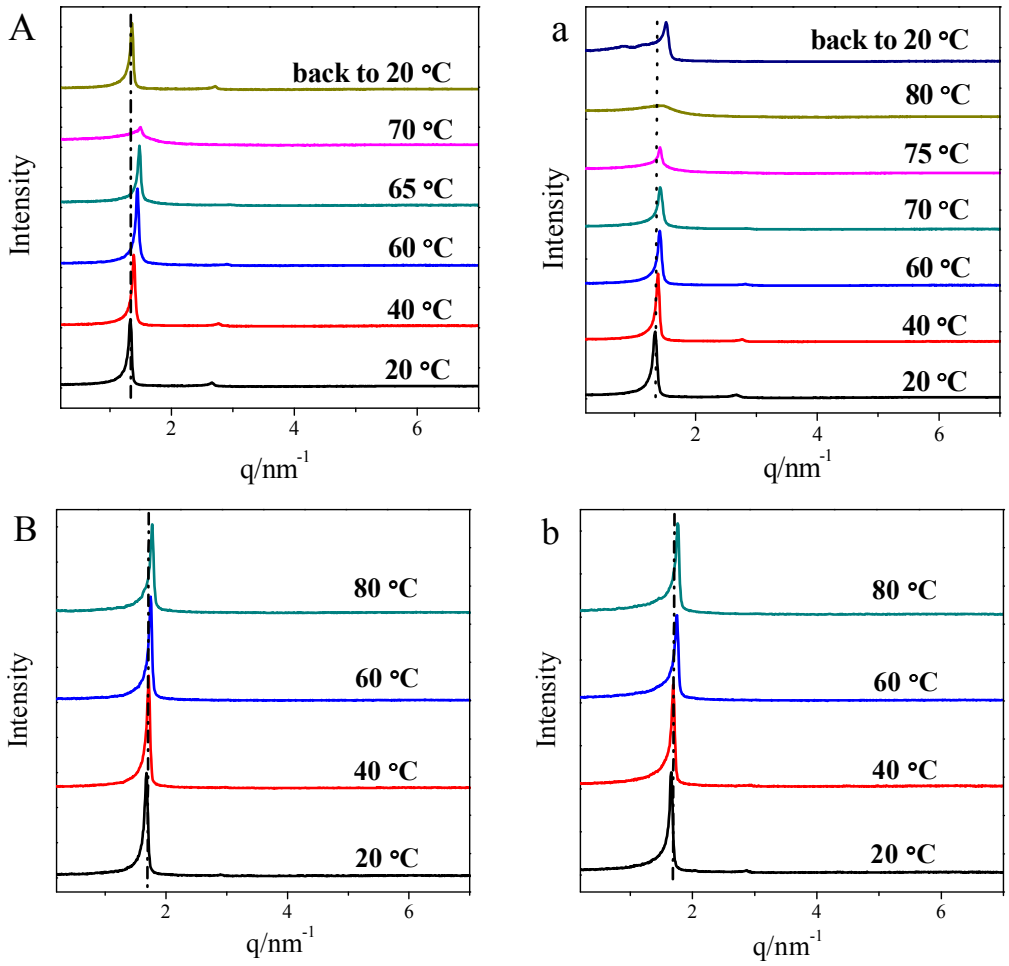


**Figure 7** The SAXS results of LLC composites (60 wt%$C_{12}E_4$/10 wt% $C_{12}$mimBr, A and a; 10 wt% $C_{12}E_4$/60 wt% $C_{12}$mimBr, B and b). The concentration of GO were 0 mg·mL$^{-1}$ (A and B) and 0.3 mg·mL$^{-1}$ (a and b).

To gain further details about the state of GO/$C_{12}E_4/C_{12}$mimBr LLC composites, POM measurements were carried out at different temperature (Figure 8). For 0.3 mg·mL$^{-1}$ GO/60 wt%

$C_{12}E_4$/10 wt% $C_{12}$mimBr LLC, maltese crosses were appeared and the aggregated GO was not found at a reunited state, which indicating that GO was well-dispersed in the $C_{12}E_4$/$C_{12}$mimBr LLC matrix at 20°C (Figure 8$A_1$). When the temperature was increased to 80°C, the texture disappeared and we observed large GO aggregates under the microscope. However, the maltese crosses texture reappeared when the temperature dropped to 20°C, but the aggregated GO was still maintained and can not recovered to the dispersed state, indicating that after the increase of the temperature, the aggregation process of GO was irreversible even the structure of $C_{12}E_4$/$C_{12}$mimBr LLC was recovered. For the hexagonal phase (0.3 mg·mL$^{-1}$ GO/10 wt% $C_{12}E_4$/60 wt% $C_{12}$mimBr LLC), when the temperature increased from 20°C to 80°C, the texture had not changed and the aggregation of GO was not occurred during the whole process of heating, indicating that the thermal stability greatly increased with the increasing of the concentration of $C_{12}$mimBr which lead GO keep a good dispersion in LLC matirx due to the stable structure.

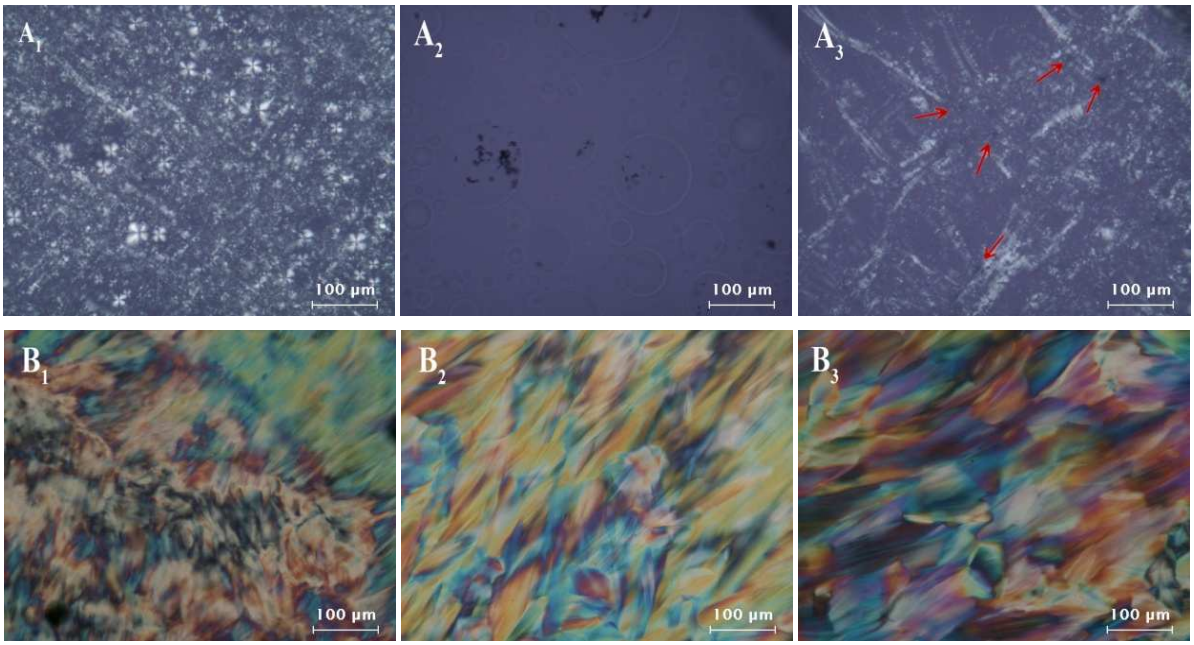


**Figure 8** POM images of liquid crystal composites as the change of temperature, $c_{GO}$=0.3 mg·mL$^{-1}$, A) 60 wt% $C_{12}E_4$/10 wt% $C_{12}$mimBr and B) 10 wt% $C_{12}E_4$/60 wt% $C_{12}$mimBr. The temperature

were $A_1$, $B_1$) 20°C, $A_2$) 80°C, $B_2$) 90°C and $A_3$, $B_3$) back to 20°C from high temperature.

Nonionic surfactants became turbid and phase separation occurred when the temperature reached above its cloud point, they are sensitive to temperature while $C_{12}$mimBr was an ionic surfactant and they did not have cloud point and the influence of temperature on their phase transition wasn't obvious. As the temperature rises, the structure of GO-$C_{12}E_4$ or GO-$C_{12}E_4$-$C_{12}$mimBr lamellar LLC composites was destroyed easily at high temperature due to its major component was $C_{12}E_4$. Then the aggregation of GO was occurred when the structure of lamellar LLC damaged and the aggregated GO can not disperse again even when the temperature recovered to room temperature and the lamellar LLC of $C_{12}E_4$ or $C_{12}E_4$/$C_{12}$mimBr recovered.

However, the addition of large amounts of $C_{12}$mimBr greatly increased the thermal stability of GO-$C_{12}E_4$-$C_{12}$mimBr hexagonal LLC and the structure of GO-$C_{12}E_4$-$C_{12}$mimBr hexagonal composites had no obvious change during the heating or cooling process because the major component was $C_{12}$mimBr in the GO-$C_{12}E_4$-$C_{12}$mimBr hexagonal LLC composites. We concluded that, the addition of $C_{12}$mimBr and GO not only can change the phase behavior of LLC but also can improve its thermal stability.

**Formation mechanism of GO/$C_{12}E_4$/$C_{12}$mimBr LLC**

Through the above results, we discussed the mechanism of the system in this paper. The experiments showed that the *d*-spacing of $C_{12}E_4$/$C_{12}$mimBr LLC composites became shorter with the concentration of $C_{12}$mimBr increasing, and there are several reasons which are shown as follow. First, it can be seen that the length of $C_{12}$mimBr (~1.9 nm) was shorter than that of $C_{12}E_4$ (~3.1 nm) (Figure 4 C), this is because that the imidazole ring of $C_{12}$mimBr is shorter than EO chain of $C_{12}E_4$. Thus, it induced the molecule of $C_{12}$mimBr is shorter than the $C_{12}E_4$ when the alkyl chain are the

same ($C_{12}$). Besides, because the imidazole ring of $C_{12}$mimBr is rigid and the EO chain of $C_{12}E_4$ is flexible, when a small amount of $C_{12}$mimBr was added to the system of $C_{12}E_4$ LLC, there are strong intermolecular hydrogen bonds interaction between EO chains and imidazole ring which induced the structure of $C_{12}E_4$/$C_{12}$mimBr LLC becoming looser compared with that of $C_{12}E_4$ LLC and the EO chains of $C_{12}E_4$ arranging around the imidazole ring of $C_{12}$mimBr and becoming bent.

Furthermore, when GO sheets were incorporated into the hydrophilic part of $C_{12}E_4$/$C_{12}$mimBr LLC matrix, because the presence of the oxygen-containing functional groups such as -COOH and -OH on the surfaces of GO, there are strong hydrogen bonds interaction between GO and EO chains or GO and imidazole ring which can enhance the mechanical property of $C_{12}E_4$/$C_{12}$mimBr LLC material. Moreover, because the *d*-spacing of $C_{12}E_4$/$C_{12}$mimBr lamellar composites is large and its structure is a little loose, thus, the addition of GO can further enlarge the hydrophilic region and increase the *d*-spacing of the GO/$C_{12}E_4$/$C_{12}$mimBr lamellar composites. But for $C_{12}E_4$/$C_{12}$mimBr hexagonal phase, because the $C_{12}E_4$/$C_{12}$mimBr hexagonal phase is a close-packed structure and the molecular arrangement is compact, therefore the GO sheets can be only well-distributed among the columns of the GO/$C_{12}E_4$/$C_{12}$mimBr hexagonal LLC composites and the *d*-spacing had no significant changes with the increase of the concentration of GO. The details of the schematic illustration of the formation of GO/$C_{12}E_4$/$C_{12}$mimBr lamellar and hexagonal LLC composites were shown in Scheme 1.

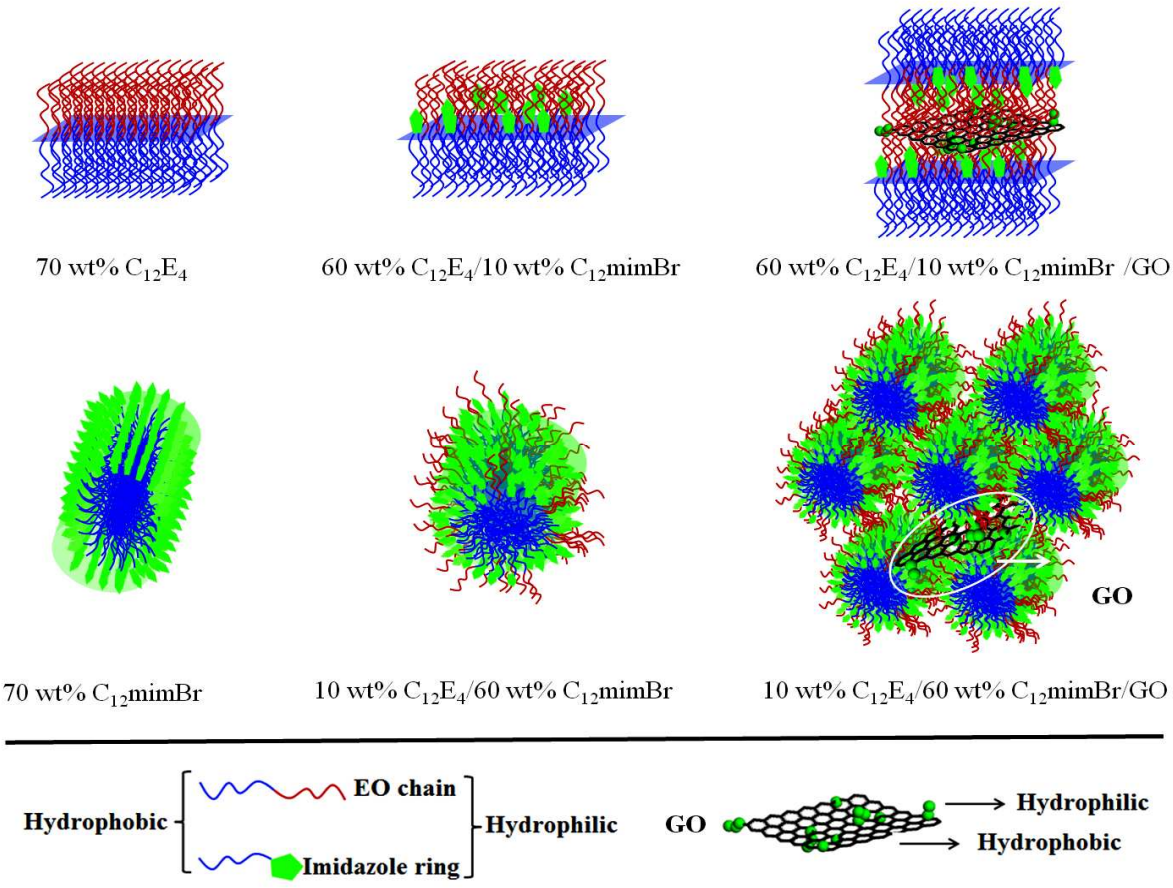


**Scheme 1** Schematic illustration of the formation of GO/$C_{12}E_4$/$C_{12}$mimBr lamellar and hexagonal LLC composites.

## Conclusions

To conclude, GO have been successfully incorporated into the lamellar and hexagonal LLC composites formed by $C_{12}E_4$ and $C_{12}$mimBr. From the experimental results, it can be observed that GO has been well-dispersed in the matrix and the additions of GO were helpful for mechanical properties of the system. Moreover, with the increase of the concentration of $C_{12}$mimBr, phase behavior of the lyotropic liquid crystals matrix changed from lamellar to hexagonal phase. It can be seen that the thermal stability of the LLC composites was greatly increased after the addition of $C_{12}$mimBr and GO into $C_{12}E_4$ LLC.

**Acknowledgements**

We gratefully acknowledge financial support from the Natural Science Foundation of China (21173128, 21203109).

**References**

1. C. L. Lester and C. A. Guymon, *Polymer*, 2002, **43**, 3707-3715.

2. B. R. Wiesenauer and D. L. Gin, *Polymer journal*, 2012, **44**, 461-468.

3. B. W. Muir, D. P. Acharya, D. F. Kennedy, X. Mulet, R. A. Evans, S. M. Pereira, K. L. Wark, B. J. Boyd, T.-H. Nguyen and T. M. Hinton, *Biomaterials*, 2012, **33**, 2723-2733.

4. W. He, Y. Fu and M. Andersson, *Journal of Materials Chemistry B*, 2014, **2**, 3214-3220.

5. X. Meng, Z. Wang, L. Wang, M. Pei, W. Guo and X. Tang, *Electronic Materials Letters*, 2013, **9**, 605-608.

6. B. S. Forney, C. l. Baguenard and C. A. Guymon, *Chemistry of Materials*, 2013, **25**, 2950-2960.

7. S. Makino, Y. Yamauchi and W. Sugimoto, *Journal of Power Sources*, 2013, **227**, 153-160.

8. M. Giese, L. K. Blusch, M. K. Khan and M. J. MacLachlan, *Angewandte Chemie International Edition*, 2015, **54**, 2888-2910.

9. N. Cheng, Q. Hu, Y. Bi, W. Xu, Y. Gong and L. Yu, *Langmuir*, 2014, **30**, 9076-9084.

10. E. Rettenmeier, A. Tokarev, C. Blanc, P. Dieudonné, Y. Guari and P. Hesemann, *Journal of colloid and interface science*, 2011, **356**, 639-646.

11. P. Brown, C. P. Butts, J. Eastoe, D. Fermin, I. Grillo, H.-C. Lee, D. Parker, D. Plana and R. M. Richardson, *Langmuir*, 2012, **28**, 2502-2509.

12. N. V. Plechkova and K. R. Seddon, *Chemical Society Reviews*, 2008, **37**, 123-150.

13. W. Kang, B. Dong, Y. Gao and L. Zheng, *Colloid and Polymer Science*, 2010, **288**, 1225-1232.

14. N. Li, S. Zhang, L. Zheng, B. Dong, X. Li and L. Yu, *Phys. Chem. Chem. Phys.*, 2008, **10**, 4375-4377.

15. L. Shi, N. Li, H. Yan, Y. a. Gao and L. Zheng, *Langmuir*, 2011, **27**, 1618-1625.

16. G. Zhang, X. Chen, Y. Zhao, Y. Xie and H. Qiu, *The Journal of Physical Chemistry B*, 2007, **111**, 11708-11713.

17. G. Zhang, X. Chen, Y. Xie, Y. Zhao and H. Qiu, *Journal of colloid and interface science*, 2007, **315**, 601-606.

18. K. Binnemans, *Chemical reviews*, 2005, **105**, 4148-4204.

19. K. Yuan, L. Chen and Y. Chen, *Chemistry-A European Journal*, 2014, **20**, 11488-11495.

20. L. Wang, X. Xin, M. Yang, X. Ma, Z. Feng, R. Chen, J. Shen and S. Yuan, *Physical Chemistry Chemical Physics*, 2014, **16**, 20932-20940.

21. S. Li, M. Fu, H. Sun, Y. Zhao, Y. Liu, D. He and Y. Wang, *The Journal of Physical Chemistry C*, 2014, **118**, 18015-18020.

22. C. Lee, X. Wei, J. W. Kysar and J. Hone, *science*, 2008, **321**, 385-388.

23. H. Kim, A. A. Abdala and C. W. Macosko, *Macromolecules*, 2010, **43**, 6515-6530.

24. C. Zhang, L. Ren, X. Wang and T. Liu, *The Journal of Physical Chemistry C*, 2010, **114**, 11435-11440.

25. Z. Xu and C. Gao, *Accounts of chemical research*, 2014, **47**, 1267-1276.

26. J. Fan, Z. Shi, M. Lian, H. Li and J. Yin, *Journal of Materials Chemistry A*, 2013, **1**, 7433-7443.

27. J. Liu, G. Liu and W. Liu, *Chemical Engineering Journal*, 2014, **257**, 299-308.

28. S. Sun and P. Wu, *Journal of Materials Chemistry*, 2011, **21**, 4095-4097.

29. X. Xin, H. Li, S. A. Wieczorek, T. Szymborski, E. Kalwarczyk, N. Ziebacz, E. Gorecka, D. Pociecha and R. Hołyst, *Langmuir*, 2009, **26**, 3562-3568.

30. X. Xin, H. Li, E. Kalwarczyk, A. Kelm, M. Fiałkowski, E. Gorecka, D. Pociecha and R. Hołyst, *Langmuir*, 2010, **26**, 8821-8828.

31. H. Bai, C. Li and G. Shi, *Advanced Materials*, 2011, **23**, 1089-1115.

32. Q. Li, X. Wang, X. Yue and X. Chen, *Langmuir*, 2014, **30**, 1522-1530.

33. X. Yue, X. Chen, Q. Li and Z. Li, *Langmuir*, 2013, **29**, 11013-11021.

34. S. Yi, Q. Li, H. Liu and X. Chen, *The Journal of Physical Chemistry B*, 2014, **118**, 11581-11590.

35. W. Xu, T. Wang, N. Cheng, Q. Hu, Y. Bi, Y. Gong and L. Yu, *Langmuir*, 2015, **31**, 1272-1282.

36. A. Anczykowska, S. Bartkiewicz, M. Nyk and J. Myśliwiec, *Applied Physics Letters*, 2011, **99**, 191109.

37. A. Babaei and A. Arefazar, *Journal of Applied Polymer Science*, 2015, **132**, 41969.

38. R. Bhargavi, G. G. Nair, S. K. Prasad, R. Majumdar and B. G. Bag, *Journal of Applied Physics*, 2014, **116**, 154902.

39. S. Song, L. Feng, A. Song and J. Hao, *The Journal of Physical Chemistry B*, 2012, **116**, 12850-12856.

40. K. P. Sharma, C. K. Choudhury, S. Srivastava, H. Davis, P. Rajamohanan, S. Roy and G. Kumaraswamy, *The Journal of Physical Chemistry B*, 2011, **115**, 9059-9069.